Observation of Antiferromagnetic Magnon Pseudospin Dynamics and the Hanle Effect

T. Wimmer,[1,2,*] A. Kamra,[3] J. Gückelhorn,[1,2] M. Opel,[1] S. Geprägs,[1] R. Gross,[1,2,4]
H. Huebl,[1,2,4] and M. Althammer[1,2,†]

[1]*Walther-Meißner-Institut, Bayerische Akademie der Wissenschaften, 85748 Garching, Germany*
[2]*Physik-Department, Technische Universität München, 85748 Garching, Germany*
[3]*Center for Quantum Spintronics, Department of Physics, Norwegian University of Science and Technology, NO-7491 Trondheim, Norway*
[4]*Munich Center for Quantum Science and Technology (MCQST), Schellingstrasse 4, D-80799 München, Germany*

(Received 31 July 2020; revised 2 October 2020; accepted 9 November 2020; published 10 December 2020)

We report on experiments demonstrating coherent control of magnon spin transport and pseudospin dynamics in a thin film of the antiferromagnetic insulator hematite utilizing two Pt strips for all-electrical magnon injection and detection. The measured magnon spin signal at the detector reveals an oscillation of its polarity as a function of the externally applied magnetic field. We quantitatively explain our experiments in terms of diffusive magnon transport and a coherent precession of the magnon pseudospin caused by the easy-plane anisotropy and the Dzyaloshinskii-Moriya interaction. This experimental observation can be viewed as the magnonic analog of the electronic Hanle effect and the Datta-Das transistor, unlocking the high potential of antiferromagnetic magnonics toward the realization of rich electronics-inspired phenomena.

DOI: 10.1103/PhysRevLett.125.247204

The different phases of electronic matter manifesting distinct transport properties are cornerstones of condensed matter physics and modern technologies. The electron spin together with spin-orbit interaction plays a fundamental role in hosting and controlling several of these phases, such as topological insulators [1,2]. Spin-dependent electronic transport has further underpinned industrial devices such as magnetoresistive read heads and memories. In these spin-electronic phenomena, the spin-orbit interaction results in an incoherent loss of spin currents but can also be exploited for coherent control of spin and its transport [3,4].

An emerging paradigm for spin and information transport via magnons in magnetic insulators offers distinct advantages [5–14]. While ferromagnetic magnons carry spin in only one direction, antiferromagnetic magnons come in pairs with opposite spins or Néel order precession chiralities. The latter can combine to form zero-spin excitations corresponding to linearly polarized oscillations of the Néel order [15,16]. In general, the pairs of antiferromagnetic magnons and their superpositions can be described via a pseudospin [17–20] in a manner similar to the actual spin of an electron [Fig. 1(a)]. Besides the unique magnonic pseudospin feature, antiferromagnets also offer crucial advantages such as immunity to stray fields [21,22], terahertz magnon frequencies [21–24], and ultrafast response times [25,26]. Within our chosen convention, the z component of such a pseudospin corresponds to the measurable magnon spin, while the transverse component characterizes the mode ellipticity and corresponds to zero-spin excitations. The formal equivalence between electron spin and antiferromagnetic magnon pseudospin has been predicted to result in a range of phenomena that are completely analogous in electronic systems and antiferromagnetic insulators (AFIs) [17–20,27–29]. The experimental realizations of these theoretical predictions promise to lift antiferromagnetic magnonics to a new level of functionalities. Here, we report the first observation of the magnonic analog of the electronic Hanle effect [30–32]. This is achieved by realizing the coherent control of the magnon spin and transport in a thin AFI.

In our experiments, spin current is injected from a heavy metal (HM) strip into an adjacent AFI via the spin Hall effect (SHE), producing an excess of spin-up magnons [11,33,34]. The injection thus creates a magnon pseudospin density directed along $\hat{z}$ [Figs. 1(b)–1(d)]. In the presence of an easy-plane anisotropy and Dzyaloshinskii-Moriya interaction (DMI), spin-up and -down magnons are coherently coupled and, therefore, no longer eigenexcitations [20,35]. As a result, the pseudospin precesses in the x-z plane with time while the magnons diffuse away from the injector. Its precession frequency Ω is determined by the anisotropy and a combination of the DMI field and canting-induced net magnetic moment. We control the latter by an external magnetic field and, hereby, obtain a handle on Ω. At the compensation field H_c, the anisotropy and the DMI contributions just cancel, resulting in $\Omega = 0$. The pseudospin, in this case, propagates through the AFI without any precession [Fig. 1(b)]. In contrast, for the field H_0, the pseudospin of the magnons arriving at the detector electrode points orthogonal to the z axis [Fig. 1(c)].

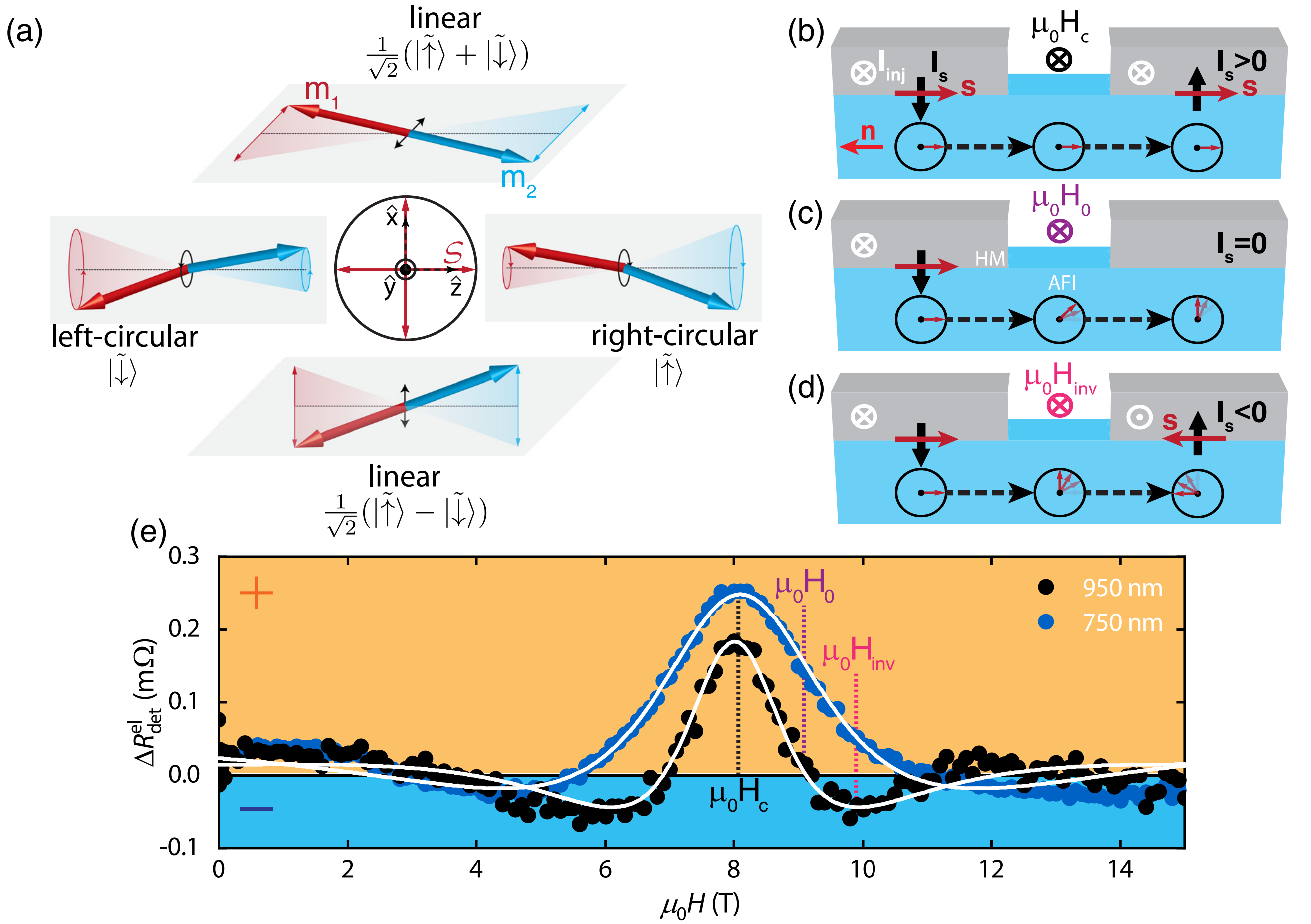

FIG. 1. (a) Pseudospin $\mathcal{S}$ description of magnonic excitations obtained by linear superpositions of spin-up and -down antiferromagnetic magnons that correspond to right- and left-circular precessions of the Néel vector $\boldsymbol{n}$, respectively. A pseudospin collinear with the z axis corresponds to spin-up or -down magnons carrying spin ± 1. As the pseudospin rotates away from the z axis, the precession of the Néel vector becomes increasingly elliptical merging into a linear oscillation for $\mathcal{S} \| \hat{x}$, corresponding to zero-spin excitations. The z component of pseudospin $\mathcal{S}_z$ determines the actual magnonic spin which is probed in our measurements. (b)–(d) Magnonic spin along $\hat{z} \| \boldsymbol{n}$ is injected and detected, respectively, by the left and right HM electrodes deposited on an AFI. The pseudospin precesses with a frequency controlled by the applied magnetic field while diffusing from the injector to the detector. As a result, positive (b), zero (c), or negative (d) magnon spin is detected giving rise to an analogous behavior of the measured spin signal between the two electrodes as shown in (e). The white curves depict the theoretical model fit [Eq. (3)] to the experimental data shown via black and blue circles for devices with an injector-detector distance of $d = 950$ nm and $d = 750$ nm, respectively, at $T = 200$ K.

This corresponds to a linearly polarized pseudospin configuration with zero magnon spin density and, thus, a vanishing magnon spin signal at the detector [Fig. 1(e)]. For H_{inv}, the magnon pseudospin and actual spin densities have reversed directions while propagating from the injector to the detector [Fig. 1(d)]. This situation corresponds to a negative magnon spin signal observed in our experiments [Fig. 1(e)].

We employ a $t = 15$ nm thin film of hematite (α-Fe_2O_3) as the AFI. Our film is characterized by an easy y-z-plane anisotropy and an out-of-plane DMI vector. The thin hematite layer features an easy-plane phase over the entire temperature range and, therefore, lacks the Morin transition [36] (see Supplemental Material for details [37]), consistent with similar films [43]. The equilibrium Néel vector $\boldsymbol{n}$ and the sublattice magnetizations $\boldsymbol{m}_{1,2}$ thus lie in the y-z plane with a small canting angle between $\boldsymbol{m}_1$ and $\boldsymbol{m}_2$ [Fig. 2(a)]. An applied magnetic field along $\hat{\boldsymbol{y}}$ orients the Néel vector along $-\hat{\boldsymbol{z}}$. The magnitude of the external magnetic field $\mu_0 H$ further controls the canting angle and the net induced magnet moment $\boldsymbol{m}_{\mathrm{net}} = \boldsymbol{m}_1 + \boldsymbol{m}_2$, both bearing a constant DMI-induced offset and a variable contribution linear in $\mu_0 H$. We use $t_{\mathrm{Pt}} = 5$-nm-thick, sputtered platinum as the HM for electrically injecting and detecting magnonic spin [7]. A charge current I_{inj} is fed through the injector featuring typical current densities of $J_{\mathrm{inj}} \sim 2 \times 10^{11}$ A/m^2. As a result, a z-polarized electron spin accumulation is generated at the interface with the AFI, leading to a z-polarized magnon spin and pseudospin current in the AFI [cf. Fig. 2(a)]. The reverse process enables the

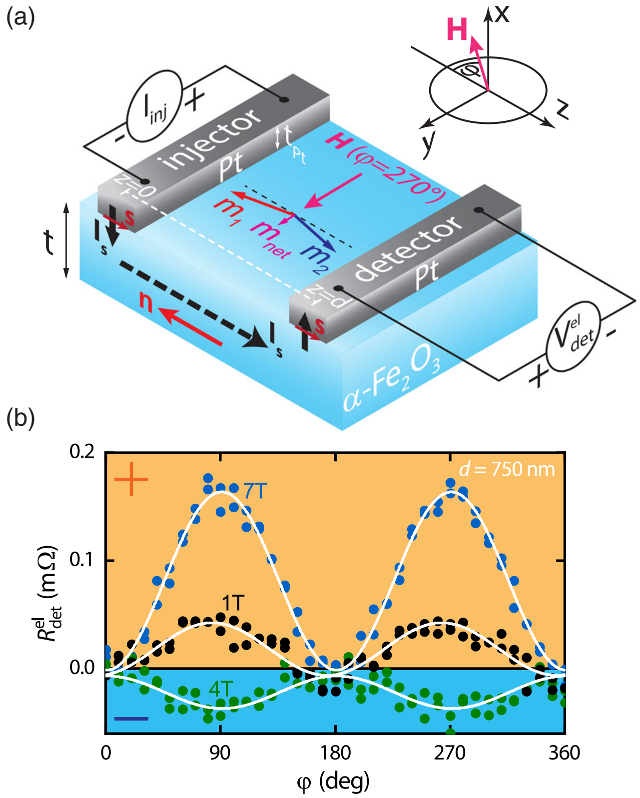

FIG. 2. (a) Sketch of the device geometry, the electrical wiring, and the coordinate system. The canting of the magnetic sublattices $\boldsymbol{m}_1$ and $\boldsymbol{m}_2$ and the corresponding net moment $\boldsymbol{m}_{\text{net}}$ as well as the Néel order parameter $\boldsymbol{n}$ are illustrated. Upon applying a charge current I_{inj} to the injector, a spin current I_s with spin polarization s is generated via the SHE and injected into the hematite (α-Fe_2O_3) with thickness t. The emerging antiferromagnetic magnon current is then detected via the inverse SHE-induced current at the detector by measuring the electrical voltage drop $V_{\text{det}}^{\text{el}}$. (b) Angle-dependent magnon spin signals $R_{\text{det}}^{\text{el}} \propto V_{\text{det}}^{\text{el}}/I_{\text{inj}}$ for electrically excited magnons measured at the detector for $T = 200$ K with a center-to-center distance of $d = 750$ nm. The white solid lines are fits to a $\sin^2(\varphi)$-type function.

detection of the magnon spin in the AFI at its interface with the detector electrode, which is measured as a charge current or voltage. We extract the electrical signals from this SHE-based magnon injection and detection scheme using the current reversal method [44,45] (see also Supplemental Material [37]).

For the configuration discussed above, the dynamics and diffusive transport of the magnon pseudospin density $\boldsymbol{\mathcal{S}}$ in the AFI is described as [46]

$$\frac{\partial \boldsymbol{\mathcal{S}}}{\partial t} = D\nabla^2 \boldsymbol{\mathcal{S}} - \frac{\boldsymbol{\mathcal{S}}}{\tau_s} + \boldsymbol{\mathcal{S}} \times \Omega \hat{\mathbf{y}}, \qquad (1)$$

in direct analogy with the spin diffusion and dynamics for itinerant electrons [30]. Here, D is the magnon diffusion constant [47], and τ_s is the spin relaxation time accounting for the incoherent effect of spin-nonconserving interactions [19]. The pseudospin precession frequency Ω characterizes the coherent effect [15,16,19] of spin-nonconserving, emergent spin-orbit [20,29] interactions that couple spin-up and -down magnon modes. For $\Omega = 0$, Eq. (1) reduces to the magnon spin transport equation for easy-axis collinear AFIs [48,49]. In contrast, easy-plane anisotropy and canting-mediated noncollinearity in our AFI films break the rotational symmetry about the Néel order and coherently couple the opposite spin magnon modes. As detailed in Supplemental Material [37], the resulting Ω is given by

$$\hbar\Omega = \hbar\omega_{\text{an}} - \mu_0 H_{\text{DMI}} m_{\text{net}} = \hbar\tilde{\omega}_{\text{an}} - \mu_0 \tilde{m} H, \qquad (2)$$

where $\tilde{\omega}_{\text{an}}$ is a normalized anisotropy frequency and H_{DMI} is the effective DMI field. $\tilde{m}$ is an equivalent magnetic moment that parametrizes the DMI strength [50]. It allows for elucidating the linear $\mu_0 H$ dependence of the noncollinearity-mediated contribution to Ω [51]. Considering z-polarized magnon spin and pseudospin current density j_{s0} injected by the electrode at $z = 0$, the steady state solution (see Supplemental Material [37]) to Eq. (1) yields for the magnon spin density $s(z) = \mathcal{S}_z(z)$

$$s(z) = \frac{j_{s0}\lambda_s}{D(a^2 + b^2)} e^{-az/\lambda_s} \left(a \cos\frac{bz}{\lambda_s} - b \sin\frac{bz}{\lambda_s} \right), \qquad (3)$$

where $a \equiv \sqrt{(1 + \sqrt{1 + \Omega^2 \tau_s^2})/2}$, $b \equiv \sqrt{(-1 + \sqrt{1 + \Omega^2 \tau_s^2})/2}$, and $\lambda_s = \sqrt{D\tau_s}$ is the spin diffusion length. Equation (3) describes the magnon spin density at a distance z from the injector. It is proportional to the magnon spin signal measured by the detector electrode at $z = d$. Together, Eqs. (2) and (3) describe the key phenomenon reported here and form the basis for analyzing our experimental data. In Fig. 1(e), corresponding theoretical curves (white solid lines) are shown together with experimental data (black and blue data points) for two devices featuring different electrode spacings d. Consistent with our model, we see a pronounced peak in the positive magnon spin signal regime for both devices. This peak corresponds to the compensation field $\mu_0 H_c$ for which $\Omega = 0$. Because of the vanishing pseudospin precession frequency at $\mu_0 H_c$, the peak position is independent of the electrode spacing d. For increasing field strength, the spin signal decreases until it approaches zero signal at $\mu_0 H_0$, corresponding to a 90° rotation of the pseudospin vector, i.e., a linear polarization of the propagating magnon modes carrying zero spin. A sign inversion of the spin signal is evident when the field is further increased to $\mu_0 H_{\text{inv}}$, corresponding to a full 180° rotation of the pseudospin vector $\boldsymbol{\mathcal{S}}$ and, therefore, an inversion of the magnon mode chirality or spin [cf. Fig. 1(a)]. Since both $\mu_0 H_0$ and $\mu_0 H_{\text{inv}}$ correspond to a finite precession frequency Ω, their values

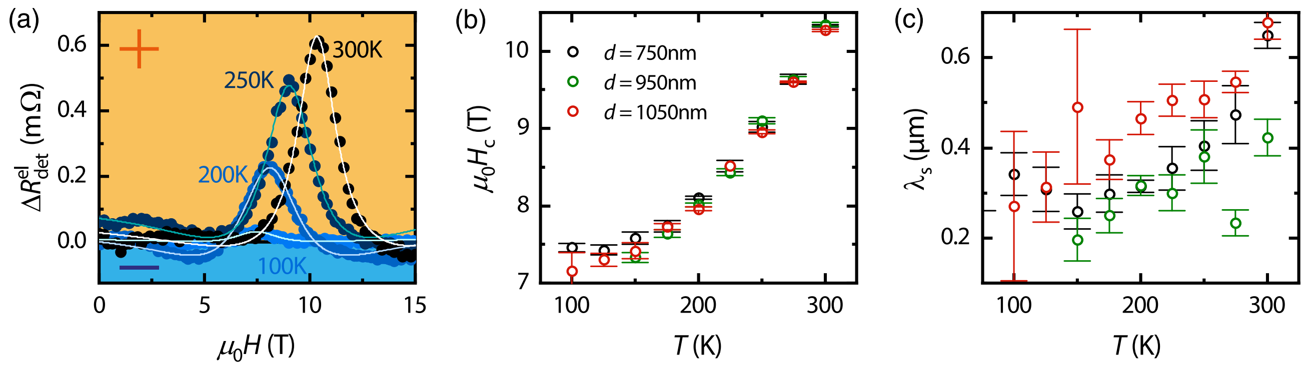

FIG. 3. (a) Electrically excited magnon spin signals $\Delta R^{el}_{det} \propto V^{el}_{det}/I_{inj}$ for a structure with strip distance $d = 750$ nm plotted as a function of the magnetic field for different temperatures. Light colored solid lines are fits to Eq. (3). (b) Compensation field $\mu_0 H_c$ versus temperature extracted from experiments with devices of varying d. The temperature dependence of $\mu_0 H_c$ follows the temperature trend of the uniaxial anisotropy of hematite. (c) Spin diffusion length λ_s as a function of the temperature extracted from experimental data from different devices with varying d. λ_s increases with increasing temperature for all investigated structures.

are expected to vary with the spacing d between the injector and detector electrodes, in agreement with our experimental data in Fig. 1(e). As evident, the same behavior is observed for decreasing field strength $\mu_0 H < \mu_0 H_c$, corresponding to a pseudospin precession in the opposite sense.

Subsequently, we measure the magnon spin signal $R^{el}_{det} \propto V^{el}_{det}/I_{inj}$ at the detector (see Supplemental Material for details [37]) as a function of the external magnetic field orientation φ within the y-z plane as illustrated in Fig. 2(a). The result is shown in Fig. 2(b) for a center-to-center strip distance of $d = 750$ nm. The data exhibit a 180°-symmetric modulation consistent with the SHE-mediated spin injection and detection of magnons [7,44]. This corresponds to a $\sin^2(\varphi)$ angular variation of the signal, which is the expected dependence for electrically induced magnon transport [7,44]. A possible spin Seebeck effect, in contrast, would yield a $\sin(\varphi)$ dependence [7,52]. Hence, the angle dependence can be fitted with a simple $\Delta R^{el}_{det} \sin^2(\varphi)$ function, where ΔR^{el}_{det} represents the amplitude of the electrical magnon spin signal. The signal modulation is shifted by ~90° compared to similar measurements on ferrimagnetic materials [7,44,53]. This is due to the fact that the electrical magnon excitation is active only when $\boldsymbol{\mu}_s \| \boldsymbol{n}$, i.e., for $\boldsymbol{H} \perp \boldsymbol{n}$ in our experiments. Thus, we can confirm that the excited magnons in our experiments originate from the antiferromagnetic Néel order consistent with previous experiments in AFIs [11]. Most importantly, we indeed observe two sign inversions of R^{el}_{det} in the investigated field range. While a positive signal is measured for $\mu_0 H = 1$ and 7 T, a negative signal ensues at 4 T. These measurements are further evidence for the rotation of the pseudospin vector via the coherent coupling Ω between the antiferromagnetic magnon modes described in the spin diffusion equation (1).

Last but not least, we extract the relevant magnon transport parameters from our data using the diffusive spin transport model given in Eq. (3). To this end, we carried out temperature-dependent measurements of the field-dependent magnon spin signals ΔR^{el}_{det}, which are shown in Fig. 3(a). Here, light colored solid lines correspond to fits to Eq. (3). For the fitting routine, we consider a finite (constant) offset signal, which is added to Eq. (3). Furthermore, the free fit parameters used were j_{s0}, λ_s, τ_s, D, and $\tilde{\omega}_{an}$, whereas $\tilde{m}$ was fixed to the value of the net magnetic moment at zero magnetic field (see Supplemental Material for details [37]). For all investigated temperatures and devices with varying d, we obtain excellent agreement between our experiments and the theoretical model, strongly supporting the validity of our theory. As evident from Fig. 3(a), we observe a decrease of the peak amplitude at $\mu_0 H_c$ with decreasing temperature, which is expected from the electrically excited magnon transport effect [44,54–56] (see also Supplemental Material [37]). Moreover, we find a clear decrease of the compensation field with decreasing temperature in Fig. 3(a). For a quantitative treatment of this behavior, we extract $\mu_0 H_c$ for each temperature from the fits (via $\tilde{\omega}_{an}$) and plot its temperature dependence in Fig. 3(b). For each structure, we observe a constant behavior in the temperature range from 100 to 150 K. A significant increase is evident for larger temperatures up to 300 K. As evident from Eq. (2), the compensation field can be expressed as $\mu_0 H_c = \hbar \tilde{\omega}_{an} (\tilde{m})^{-1}$. Therefore, $\mu_0 H_c$ directly corresponds to the normalized anisotropy energy $\tilde{\omega}_{an}$ of the hematite. We thus expect that $\mu_0 H_c$ follows the temperature dependence of the easy-plane anisotropy. This is supported by previous measurements of the temperature dependence of the anisotropy energy in hematite, which qualitatively agree with the temperature dependence of $\mu_0 H_c$ [57]. Hence, our results support the assumption that the coupling strength Ω defined in Eq. (2) is related to the easy-plane anisotropy in hematite. Finally, we calculate the magnon diffusion length λ_s using the extracted diffusion constant D and the spin relaxation time τ_s from our fits. The obtained temperature dependence of λ_s

is shown in Fig. 3(c). Overall, we find an increase of λ_s with increasing temperature for all studied injector-detector distances d. At room temperature, we extract $\lambda_s \approx 0.5\ \mu$m, which is in perfect agreement with recent reports measuring the spin diffusion length in the easy-plane phase of hematite thin films using distance-dependent measurements [43,58].

As a key result, we have experimentally demonstrated the coherent control of spin currents and magnon pseudospin dynamics in antiferromagnetic insulators. This opens new avenues for antiferromagnetic magnonic applications such as spin-based transistors or field-controlled switchable devices. Moreover, our experimental exploitation of the magnonic equivalent of a spin-$1/2$ electron system provides the first crucial step toward various pseudospin-based concepts such as an unconventional non-Abelian computing scheme [18].

We gratefully acknowledge financial support from the Deutsche Forschungsgemeinschaft (DFG, German Research Foundation) under Germany's Excellence Strategy EXC-2111-390814868 and Project No. AL2110/2-1 and the Research Council of Norway through its Centers of Excellence funding scheme, Project No. 262633, "QuSpin." A. K. thanks Siddhartha Omar for valuable discussions.

Note added.—A similar magnon Hanle effect signal has also been observed in Zn-doped Hematite recently [59]. A significantly different magnetic free energy landscape of the latter material, as compared to our undoped films, demonstrates the potentially broad platforms where the magnon Hanle effect plays an important role.

*tobias.wimmer@wmi.badw.de
†matthias.althammer@wmi.badw.de

[1] M. Z. Hasan and C. L. Kane, Colloquium: Topological insulators, Rev. Mod. Phys. **82**, 3045 (2010).
[2] Y. Tokura, K. Yasuda, and A. Tsukazaki, Magnetic topological insulators, Nat. Rev. Phys. **1**, 126 (2019).
[3] S. Datta and B. Das, Electronic analog of the electro-optic modulator, Appl. Phys. Lett. **56**, 665 (1990).
[4] A. Manchon, J. Železný, I. M. Miron, T. Jungwirth, J. Sinova, A. Thiaville, K. Garello, and P. Gambardella, Current-induced spin-orbit torques in ferromagnetic and antiferromagnetic systems, Rev. Mod. Phys. **91**, 035004 (2019).
[5] G. E. W. Bauer, E. Saitoh, and B. J. van Wees, Spin caloritronics, Nat. Mater. **11**, 391 (2012).
[6] A. V. Chumak, V. I. Vasyuchka, A. A. Serga, and B. Hillebrands, Magnon spintronics, Nat. Phys. **11**, 453 (2015).
[7] L. J. Cornelissen, J. Liu, R. A. Duine, J. Ben Youssef, and B. J. van Wees, Long-distance transport of magnon spin information in a magnetic insulator at room temperature, Nat. Phys. **11**, 1022 (2015).
[8] K. Nakata, P. Simon, and D. Loss, Spin currents and magnon dynamics in insulating magnets, J. Phys. D **50**, 114004 (2017).
[9] W. Yuan, Q. Zhu, T. Su, Y. Yao, W. Xing, Y. Chen, Y. Ma, X. Lin, J. Shi, R. Shindou, X. C. Xie, and W. Han, Experimental signatures of spin superfluid ground state in canted antiferromagnet Cr2O3 via nonlocal spin transport, Sci. Adv. **4**, eaat1098 (2018).
[10] M. Althammer, Pure spin currents in magnetically ordered insulator/normal metal heterostructures, J. Phys. D **51**, 313001 (2018).
[11] R. Lebrun, A. Ross, S. A. Bender, A. Qaiumzadeh, L. Baldrati, J. Cramer, A. Brataas, R. A. Duine, and M. Kläui, Tunable long-distance spin transport in a crystalline antiferromagnetic iron oxide, Nature (London) **561**, 222 (2018).
[12] D. Hou, Z. Qiu, and E. Saitoh, Spin transport in antiferromagnetic insulators: Progress and challenges, NPG Asia Mater. **11**, 35 (2019).
[13] T. Wimmer, M. Althammer, L. Liensberger, N. Vlietstra, S. Geprägs, M. Weiler, R. Gross, and H. Huebl, Spin Transport in a Magnetic Insulator with Zero Effective Damping, Phys. Rev. Lett. **123**, 257201 (2019).
[14] A. Kamra, E. Thingstad, G. Rastelli, R. A. Duine, A. Brataas, W. Belzig, and A. Sudbø, Antiferromagnetic magnons as highly squeezed Fock states underlying quantum correlations, Phys. Rev. B **100**, 174407 (2019).
[15] A. Kamra, U. Agrawal, and W. Belzig, Noninteger-spin magnonic excitations in untextured magnets, Phys. Rev. B **96**, 020411(R) (2017).
[16] L. Liensberger, A. Kamra, H. Maier-Flaig, S. Geprägs, A. Erb, S. T. B. Goennenwein, R. Gross, W. Belzig, H. Huebl, and M. Weiler, Exchange-Enhanced Ultrastrong Magnon-Magnon Coupling in a Compensated Ferrimagnet, Phys. Rev. Lett. **123**, 117204 (2019).
[17] R. Cheng, M. W. Daniels, J.-G. Zhu, and D. Xiao, Antiferromagnetic spin wave field-effect transistor, Sci. Rep. **6**, 24223 (2016).
[18] M. W. Daniels, R. Cheng, W. Yu, J. Xiao, and D. Xiao, Nonabelian magnonics in antiferromagnets, Phys. Rev. B **98**, 134450 (2018).
[19] K. Shen, Magnon Spin Relaxation and Spin Hall Effect Due to the Dipolar Interaction in Antiferromagnetic Insulators, Phys. Rev. Lett. **124**, 077201 (2020).
[20] M. Kawano and C. Hotta, Thermal hall effect and topological edge states in a square-lattice antiferromagnet, Phys. Rev. B **99**, 054422 (2019).
[21] T. Jungwirth, X. Marti, P. Wadley, and J. Wunderlich, Antiferromagnetic spintronics, Nat. Nanotechnol. **11**, 231 (2016).
[22] V. Baltz, A. Manchon, M. Tsoi, T. Moriyama, T. Ono, and Y. Tserkovnyak, Antiferromagnetic spintronics, Rev. Mod. Phys. **90**, 015005 (2018).
[23] J. Li, C. B. Wilson, R. Cheng, M. Lohmann, M. Kavand, W. Yuan, M. Aldosary, N. Agladze, P. Wei, M. S. Sherwin, and J. Shi, Spin current from sub-terahertz-generated antiferromagnetic magnons, Nature (London) **578**, 70 (2020).
[24] P. Vaidya, S. A. Morley, J. van Tol, Y. Liu, R. Cheng, A. Brataas, D. Lederman, and E. del Barco, Subterahertz spin

pumping from an insulating antiferromagnet, Science **368**, 160 (2020).

[25] P. Němec, M. Fiebig, T. Kampfrath, and A. V. Kimel, Antiferromagnetic opto-spintronics, Nat. Phys. **14**, 229 (2018).

[26] K. Olejník, T. Seifert, Z. Kašpar, V. Novák, P. Wadley, R. P. Campion, M. Baumgartner, P. Gambardella, P. Němec, J. Wunderlich, J. Sinova, P. Kužel, M. Müller, T. Kampfrath, and T. Jungwirth, Terahertz electrical writing speed in an antiferromagnetic memory, Sci. Adv. **4**, eaar3566 (2018).

[27] R. Cheng, S. Okamoto, and D. Xiao, Spin Nernst Effect of Magnons in Collinear Antiferromagnets, Phys. Rev. Lett. **117**, 217202 (2016).

[28] V. A. Zyuzin and A. A. Kovalev, Magnon Spin Nernst Effect in Antiferromagnets, Phys. Rev. Lett. **117**, 217203 (2016).

[29] M. Kawano, Y. Onose, and C. Hotta, Designing Rashba-Dresselhaus effect in magnetic insulators, Commun. Phys. **2**, 27 (2019).

[30] J. Fabian, A. Matos-Abiague, C. Ertler, P. Stano, and I. Zutic, Semiconductor spintronics, Acta Phys. Slovaca **57**, 565 (2007).

[31] J. M. Kikkawa and D. D. Awschalom, Lateral drag of spin coherence in gallium arsenide, Nature (London) **397**, 139 (1999).

[32] F. J. Jedema, H. B. Heersche, A. T. Filip, J. J. A. Baselmans, and B. J. van Wees, Electrical detection of spin precession in a metallic mesoscopic spin valve, Nature (London) **416**, 713 (2002).

[33] S. Takei and Y. Tserkovnyak, Superfluid Spin Transport Through Easy-Plane Ferromagnetic Insulators, Phys. Rev. Lett. **112**, 227201 (2014).

[34] J. Sinova, S. O. Valenzuela, J. Wunderlich, C. H. Back, and T. Jungwirth, Spin Hall effects, Rev. Mod. Phys. **87**, 1213 (2015).

[35] S. M. Rezende, A. Azevedo, and R. L. Rodríguez-Suárez, Introduction to antiferromagnetic magnons, J. Appl. Phys. **126**, 151101 (2019).

[36] F. J. Morin, Magnetic susceptibility of αfe_2o_3 and αfe_2o_3 with added titanium, Phys. Rev. **78**, 819 (1950).

[37] See Supplemental Material at http://link.aps.org/supplemental/10.1103/PhysRevLett.125.247204, which includes Refs. [38–42], for details on growth conditions and magnetometry measurements of our hematite films, details on the measurement technique and geometry of the nanostructures, a rigorous description of the fitting routine of the field-dependent magnon spin signals, a more detailed study of the temperature-dependent magnon spin signals, and a verification of the linearity of the current-voltage characteristics of the magnon spin signals, as well as measurements ruling out electric leakage currents between the injector and the detector electrode. Additionally, we present a detailed description of the diffusive spin transport theory including the antiferromagnetic pseudospin dynamics.

[38] R. Nathans, S. J. Pickart, H. A. Alperin, and P. J. Brown, Polarized-neutron study of hematite, Phys. Rev. **136**, A1641 (1964).

[39] J. C. Marmeggi, D. Hohlwein, and E. F. Bertaut, Magnetic neutron Laue diffraction study of the domain distribution in α-fe_2o_3, Phys. Status Solidi (a) **39**, 57 (1977).

[40] J. A. Eaton and A. H. Morrish, Magnetic domains in hematite at and above the Morin transition, J. Appl. Phys. **40**, 3180 (1969).

[41] A. Ross, R. Lebrun, O. Gomonay, D. A. Grave, A. Kay, L. Baldrati, S. Becker, A. Qaiumzadeh, C. Ulloa, G. Jakob, F. Kronast, J. Sinova, R. Duine, A. Brataas, A. Rothschild, and M. Kläui, Propagation length of antiferromagnetic magnons governed by domain configurations, Nano Lett. **20**, 306 (2020).

[42] R. A. Lefever, 1.1.2 hematite alpha-Fe2O3 and hematite with substitutions, in *Landolt-Börnstein—Group III Condensed Matter* (Springer-Verlag, Berlin, 1970), pp. 8–16.

[43] J. Han, P. Zhang, Z. Bi, Y. Fan, T. S. Safi, J. Xiang, J. Finley, L. Fu, R. Cheng, and L. Liu, Birefringence-like spin transport via linearly polarized antiferromagnetic magnons, Nat. Nanotechnol. **15**, 563 (2020).

[44] S. T. B. Goennenwein, R. Schlitz, M. Pernpeintner, K. Ganzhorn, M. Althammer, R. Gross, and H. Huebl, Non-local magnetoresistance in YIG/Pt nanostructures, Appl. Phys. Lett. **107**, 172405 (2015).

[45] K. Ganzhorn, S. Klingler, T. Wimmer, S. Geprägs, R. Gross, H. Huebl, and S. T. B. Goennenwein, Magnon-based logic in a multi-terminal YIG/pt nanostructure, Appl. Phys. Lett. **109**, 022405 (2016).

[46] A. Kamra, T. Wimmer, H. Huebl, and M. Althammer, Antiferromagnetic magnon pseudospin: Dynamics and diffusive transport, Phys. Rev. B **102**, 174445 (2020).

[47] L. J. Cornelissen, K. J. H. Peters, G. E. W. Bauer, R. A. Duine, and B. J. van Wees, Magnon spin transport driven by the magnon chemical potential in a magnetic insulator, Phys. Rev. B **94**, 014412 (2016).

[48] K. Shen, Pure spin current in antiferromagnetic insulators, Phys. Rev. B **100**, 094423 (2019).

[49] R. E. Troncoso, S. A. Bender, A. Brataas, and R. A. Duine, Spin transport in thick insulating antiferromagnetic films, Phys. Rev. B **101**, 054404 (2020).

[50] A. H. Morrish, *Canted Antiferromagnetism: Hematite* (World Scientific, Singapore, 1995).

[51] In general, Ω is expected to bear a constant contribution from anisotropy and a canting-mediated contribution that depends on the applied field $\mu_0 H$. These will differ for different materials and crystal structures, and Ω versus $\mu_0 H$ may be considered a Taylor expansion.

[52] K. Ganzhorn, T. Wimmer, J. Cramer, R. Schlitz, S. Geprägs, G. Jakob, R. Gross, H. Huebl, M. Kläui, and S. T. B. Goennenwein, Temperature dependence of the non-local spin Seebeck effect in YIG/Pt nanostructures, AIP Adv. **7**, 085102 (2017).

[53] J. Shan, P. Bougiatioti, L. Liang, G. Reiss, T. Kuschel, and B. J. van Wees, Nonlocal magnon spin transport in $NiFe_2O_4$ thin films, Appl. Phys. Lett. **110**, 132406 (2017).

[54] L. J. Cornelissen, J. Shan, and B. J. van Wees, Temperature dependence of the magnon spin diffusion length and magnon spin conductivity in the magnetic insulator yttrium iron garnet, Phys. Rev. B **94**, 180402(R) (2016).

[55] K. Chen, W. Lin, C. L. Chien, and S. Zhang, Temperature dependence of angular momentum transport across interfaces, Phys. Rev. B **94**, 054413 (2016).

[56] J. Fontcuberta, H. B. Vasili, J. Gàzquez, and F. Casanova, On the role of interfaces on spin transport in magnetic

insulator/normal metal heterostructures, Adv. Mater. Interfaces **6**, 1900475 (2019).

[57] P. J. Besser, A. H. Morrish, and C. W. Searle, Magnetocrystalline anisotropy of pure and doped hematite, Phys. Rev. **153**, 632 (1967).

[58] R. Lebrun, A. Ross, O. Gomonay, V. Baltz, U. Ebels, A. L. Barra, A. Qaiumzadeh, A. Brataas, J. Sinova, and M. Kläui, Long-distance spin-transport across the Morin phase transition up to room temperature in the ultra-low damping alpha-fe2o3 antiferromagnet, arXiv:2005.14414.

[59] A. Ross, R. Lebrun, L. Baldrati, A. Kamra, O. Gomonay, S. Ding, F. Schreiber, D. Backes, F. Maccherozzi, D. A. Grave, A. Rothschild, J. Sinova, and M. Kläui, An insulating doped antiferromagnet with low magnetic symmetry as a room temperature spin conduit, arXiv:2011.09755.